Possible Quantum Paramagnetism in Compressed Sr_2IrO_4

D. Haskel[1,*] G. Fabbris[1,†] J. H. Kim,[1] L. S. I. Veiga,[1,2,3,4] J. R. L. Mardegan,[1,3] C. A. Escanhoela, Jr.,[1,2] S. Chikara[1]
V. Struzhkin,[5] T. Senthil,[6] B. J. Kim,[7,8] G. Cao,[9] and J.-W. Kim[1]

[1]*Advanced Photon Source, Argonne National Laboratory, Argonne, Illinois 60439, USA*
[2]*Brazilian Synchrotron Light Laboratory (LNLS), Campinas, São Paulo 13083-970, Brazil*
[3]*Instituto de Física Gleb Wataghin, Universidade Estadual de Campinas, Campinas, São Paulo 13083-859, Brazil*
[4]*London Centre for Nanotechnology and Department of Physics and Astronomy, University College London,
Gower Street, London, WC1E 6BT, United Kingdom*
[5]*Geophysical Laboratory, Carnegie Institution of Washington, Washington, DC 20015, USA*
[6]*Department of Physics, Massachusetts Institute of Technology, Cambridge, Massachusetts 02139, USA*
[7]*Center for Artificial Low Dimensional Electronic Systems, Institute for Basic Science (IBS),
77 Cheongam-Ro, Pohang 790-784, South Korea*
[8]*Department of Physics, Pohang University of Science and Technology, Pohang 790-784, South Korea*
[9]*Department of Physics, University of Colorado, Boulder, Colorado 80309, USA*

The effect of compression on the magnetic ground state of Sr_2IrO_4 is studied with x-ray resonant techniques in the diamond anvil cell. The weak interlayer exchange coupling between square-planar 2D IrO_2 layers is readily modified upon compression, with a crossover between magnetic structures around 7 GPa mimicking the effect of an applied magnetic field at ambient pressure. Higher pressures drive an order-disorder magnetic phase transition with no magnetic order detected above 17–20 GPa. The persistence of strong exchange interactions between $J_{eff} = 1/2$ magnetic moments within the insulating IrO_2 layers up to at least 35 GPa points to a highly frustrated magnetic state in compressed Sr_2IrO_4, opening the door for realization of novel quantum paramagnetic phases driven by extended $5d$ orbitals with entangled spin and orbital degrees of freedom.

The sizable spin-orbit interaction acting on $5d$ electrons of heavy transition metal ions, together with the large spatial extent of $5d$ orbitals and the related reduction (enhancement) of Coulomb (crystal field) interactions, leads to the emergence of novel exotic ground states in some of their oxide forms, chief among them tetravalent iridium compounds with half-filled $5d$ bands and $J_{eff} = \frac{1}{2}$ states [1–14]. Most notably, bond-directional exchange anisotropy arising from spin-orbit coupling is expected to enhance frustration in honeycomb [1,15] and triangular-kagome lattices [16–18], leading to novel quantum spin-liquid (QSL) ground states [19], such as the one predicted by Kitaev [20]. The square lattice of Sr_2IrO_4 (Sr-214) is also capable of harboring frustration and quantum paramagnetic phases, e.g., within the $J_1 - J_2 - J_3$ model [21–26] if second and/or third neighbor exchange interactions become a sizable fraction of, and compete with, first neighbor exchange interactions. The connection between QSLs and superconductivity in square lattices, via the resonating valence bond model of Anderson [27], raises prospects that new forms of superconductivity could be found in iridates [9]. In fact, the single layer Sr-214 is nearly isostructural and displays the same spectrum of magnetic excitations as the La_2CuO_4 parent compound of high-T_c cuprates [28,29],

and recent doping experiments reinforce this connection [7,8].

Since magnetically ordered and quantum paramagnetic phases (such as spin liquids [22,27,30,31] and valence bond solids [32]) compete for spin-spin correlations in space and time, it seems desirable to continuously tune competing exchange interactions with pressure in order to suppress magnetic order, without the need for chemical substitutions and unwanted lattice disorder. Pressure has recently been used to drive honeycomb iridates away from magnetically ordered states [15,33–35], although observation of dimerized phases driven by formation of Ir_2 molecular orbitals across edge-shared IrO_6 octahedra [36–38] highlights the complexity and diversity of accessible magnetic ground states in compressed lattices. The rigid network of corner-shared IrO_6 octahedra underlying the square lattice of Sr-214 is robust against Ir dimerization and provides a suitable platform for continuously tuning exchange interactions while preserving crystal structure.

In this Letter, we report on the use of pressure to tune exchange interactions in Sr-214 and drive it into what appears to be a quantum paramagnetic state. Using x-ray resonant magnetic scattering (XRMS) and x-ray magnetic circular dichroism (XMCD) measurements in the diamond
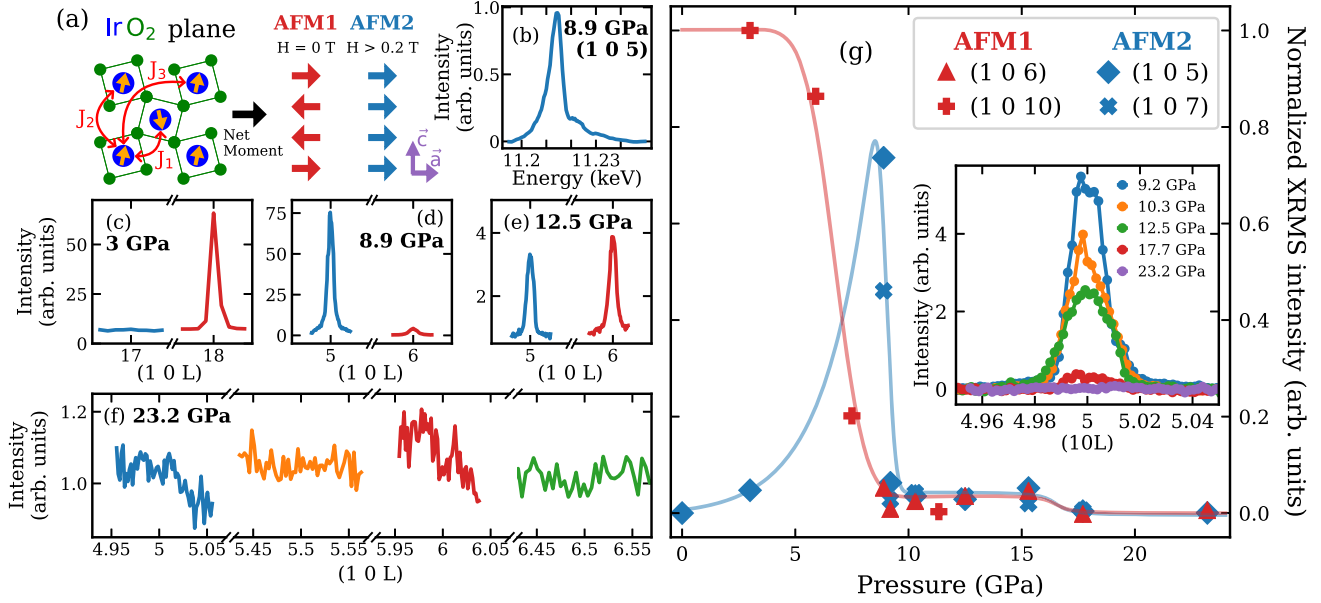
FIG. 1.   (a) Schematic of the in-plane magnetic arrangement in Sr-214 at ambient pressure. Iridium (oxygen) ions are shown in blue (green). $J_{1,2,3}$ denote first, second, and third neighbor exchange constants. The c-axis stacking of net magnetic moments in IrO_2 layers in zero field (AFM1 order) and applied field (AFM2 order) [5] is also shown. (b) Resonance enhancement of the (1 0 5) magnetic peak across the Ir L_3 edge ($2p_{3/2} \to 5d$, $E = 11.215$ keV) for $P = 8.9$ GPa, $T = 10$ K. (c)–(f) Pressure-dependent single crystal resonant diffraction from selected (1 0 L) magnetic reflections measured in transmission (Laue) geometry at $T = 10$ K in zero field (neon pressure medium). Magnetic intensities are normalized to those of (1 1 10) lattice peak. Peak count rates at magnetic (1 0 5), (1 0 6), and lattice (1 1 10) peaks for $P = 8.9$ GPa, $T = 10$ K are 2.4×10^5, 7.2×10^3, and 2.8×10^8 photons/s, respectively. Reflections in (c)–(e) showed typical resonant enhancement as in (b), while no enhancement was observed in residual background shown in (f). (g) Integrated intensities of selected magnetic peaks normalized to those of nearby (1 1 10) lattice peak. The solid lines are guides. (Inset) Evolution of (1 0 5) integrated intensity at selected pressures ($T = 10$ K). A crossover between magnetic structures takes place at $P \sim 7$ GPa, followed by coexistence and continuous suppression of magnetic order with no detectable magnetic scattering at $\sim$23 GPa, as seen in this inset.

anvil cell, we were able to probe the evolution of both the antiferromagnetic (AFM) structure in reciprocal space (in zero applied field) and the weak ferromagnetic (W-FM) response in applied field across a critical pressure $P_c \sim$ 17–20 GPa where magnetic order vanishes. XMCD measurements of the magnetic susceptibility in the putative quantum paramagnetic phase indicate that strong local AFM exchange interactions remain present to at least 35 GPa with a Curie-Weiss temperature $\theta_{CW} = -209(40)$ K, despite the lack of discernible magnetic order down to $T = 1.6$ K even in large applied field $H = 6$ T, indicative of a high degree of frustration within the IrO_2 2D layers. The exciting prospect of a quantum critical point separating Néel order and quantum paramagnetic phases in compressed Sr-214 underpins the need for theoretical and experimental efforts aimed at understanding how frustration of magnetic interactions emerges in square lattices with extended $5d$ orbitals and entangled spin and orbital degrees of freedom.

The magnetic structure of Sr_2IrO_4 at ambient pressure has been determined by both x-ray [5] and neutron [39] diffraction. The predominant Ir-O-Ir superexchange interaction ($J_1 = 60$ meV [28]) combined with the Dzyaloshinsky-Moriya (D-M) interaction [40,41] drive a canted antiferromagnetic arrangement within the IrO_2 layer [Fig. 1(a)].

The ground state magnetic structure features an alternating stacking pattern along the c axis [AFM1, Fig. 1(a)] giving rise to $(1,0,4n+2)$ magnetic reflections [5]. A modest applied field (> 0.2 T) is sufficient to modify the weak interlayer coupling (0.6 meV [42]) and give rise to a Zeeman-energy-driven ferromagnetic stacking sequence of net moments along the c axis [AFM2, Fig. 1(a)], $(1,0,2n+1)$ magnetic reflections, and weak ferromagnetism 0.05–$0.075 \mu_B$/Ir [5,43].

The evolution of the magnetic structure with pressure probed by XRMS in zero applied field and $T = 10$ K is shown in Figs. 1(c)–1(g). Details on the experimental setup are found in the Supplemental Material [44]. A dramatic crossover between AFM1 and AFM2 magnetic structures takes place around 7(1) GPa [Fig. 1(g)]. Pressure then, at first, mimics the effect of an applied field, a modest c-axis compression $\sim$0.9% at 7 GPa [58,59] having a dramatic effect on the interlayer exchange interactions. While the AFM2 phase is stabilized in a narrow pressure range around 8 GPa at the expense of the AFM1 phase, a strong suppression of the XRMS intensity from either phase is observed above $\sim$9 GPa ($\times$25 intensity reduction at 10 GPa). Further pressure causes the weak XRMS intensities from coexisting phases to vanish at about 18 GPa

[Fig. 1(f)]. The absence of magnetic Bragg peaks at L and $L + \frac{1}{2}$ for odd and even L values points to the suppression of magnetic order. In particular, this observation negates the presence of collinear in-plane AFM order, as such state would lead to (1, 0, even) magnetic peaks as observed in Ba_2IrO_4 [61,62]. This conclusion is also supported by the persistent IrO_6 rotations at high pressures [44]. Despite possible evidence for an increased tetragonal distortion of IrO_6 octahedra [58,59], the absence of (1, 0, odd) magnetic peaks also discards a spin-flop transition into a c-axis collinear AFM structure [11], as seen in Mn-doped Sr-214 [63].

Despite the strong in-plane exchange interaction, 3D magnetic order in Sr_2IrO_4 is stabilized at ambient pressure by the weak interlayer coupling. Thus, the observed collapse of 3D magnetic order at high pressures could be attributed to a frustrated interlayer coupling. However, in such case, one would expect an applied magnetic field to lift such frustration and drive magnetic order. To address this possibility, we constructed an Ir L_3 XMCD (P, T) phase diagram by collecting data in an applied field for selected isotherms [Fig. 2(a)]. A modest magnetic field $H = 0.5$ T stabilizes the AFM2 phase at low pressures and temperatures, leading to a measurable XMCD signal that is proportional to the Ir magnetization [58]. The pressure range between 10 and 15 GPa is particularly noteworthy [$P/P_0 = 0.52$–0.78 in Fig. 2(b), $P_0 = 19.2$ GPa], since a large drop of the zero field XRMS intensity in this pressure range [Fig. 1(g)] is contrasted by a small reduction of the $H = 0.5$ T XMCD signal ($\lesssim 30\%$), emphasizing the ability of a magnetic field to drive 3D magnetic order in Sr-214 even in the presence of frustrated interlayer coupling. Therefore, the combined collapse of XMCD and XRMS signals beyond 18–20 GPa is compelling evidence that such magnetic transition fundamentally involves the magnetism and/or magnetic interactions within the IrO_2 layers. The evolution of magnetization with pressure at 11 K plotted vs reduced pressure P/P_0 maps to that of the temperature-induced order-disorder transition at 1 bar [Fig. 2(b), $T_0 = 250$ K] pointing to second-order character, which is also seen in a gradual reduction of T_N with pressure [Fig. 2(a)]. This behavior is consistent with evolution toward a quantum critical point, but inconsistent with a transition into incommensurate spiral or other unconventional phases with different magnetic symmetry, expected to be first order. Furthermore, the consistent critical pressures P_0 for single crystalline and polycrystalline samples, together with lattice strain values below about 0.1% at 23 GPa [44], rule out lattice disorder as the primary driver for the magnetic transition.

Having established the absence of magnetic order in Sr-214 at high pressures, we now provide evidence in support of a pressure-induced magnetically disordered phase driven by in-plane quantum fluctuations (i.e., a quantum paramagnet). To this end, we studied the magnetic
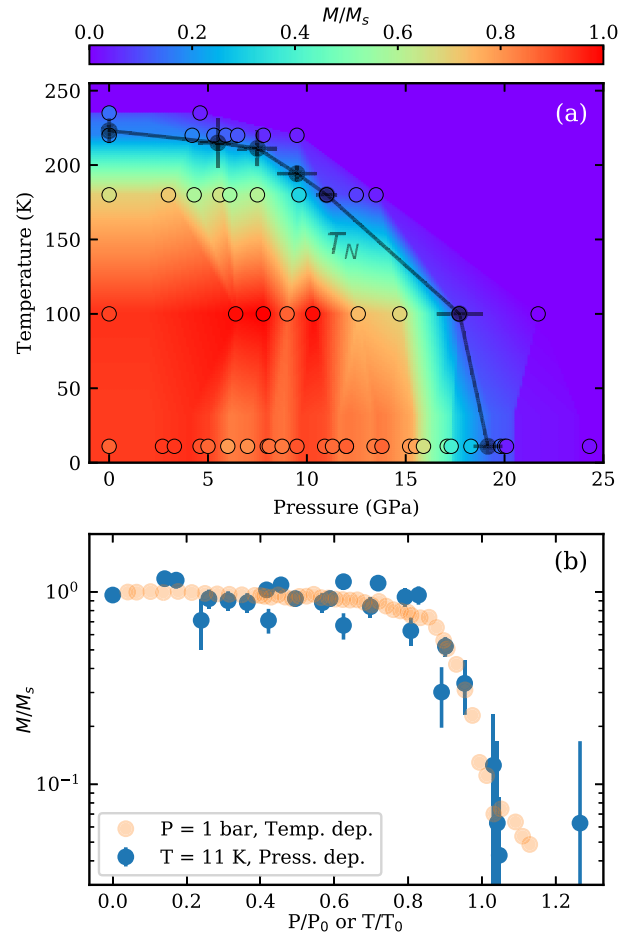

FIG. 2. (a) Pressure-temperature evolution of Ir magnetization in $H = 0.5$ T applied field for a powder sample of Sr_2IrO_4 (ground single crystal) in neon pressure medium. Circles denote P/T values at which XMCD data were collected along isotherms. Color scale represents net magnetization normalized to saturation $M_s(P = 1 \text{ bar}, T = 5.6 \text{ K})$. Unity corresponds to 3% XMCD signal and net moment 0.05 μ_B/Ir. The Néel temperature T_N at selected pressures, shown by solid black circles, was obtained by constraining $M(T)$ to its functional form at ambient pressure. (b) Magnetization plotted as function of reduced pressure P/P_0 ($T = 11$ K, $H = 0.5$ T, $P_0 = 19.2$ GPa) and reduced temperature T/T_0 ($P = 1$ bar, $H = 0.8$ T, $T_0 = 250$ K).

field (up to 6 T) and temperature dependence of the Ir L_3 XMCD at 25 and 35 GPa. Despite a substantial reduction in XMCD intensity beyond 17 GPa, a small signal is observed in large magnetic fields [Fig. 3(a)]. Noticeably, the room temperature magnetic response is pressure independent up to at least 35 GPa [Fig. 3(c)], demonstrating that the local Ir magnetic moment is preserved in this pressure range. Combined with the persistent insulating state and nearly constant $\langle \mathbf{L} \cdot \mathbf{S} \rangle$ [58,64], this result establishes that Sr-214 remains a $J_{\text{eff}} = \frac{1}{2}$-like Mott insulator at least up to 35 GPa.

The temperature dependence of the XMCD intensity shows the absence of magnetic order down to $T = 1.6$ K even in an $H = 6$ T applied field [Fig. 3(c)]. As discussed
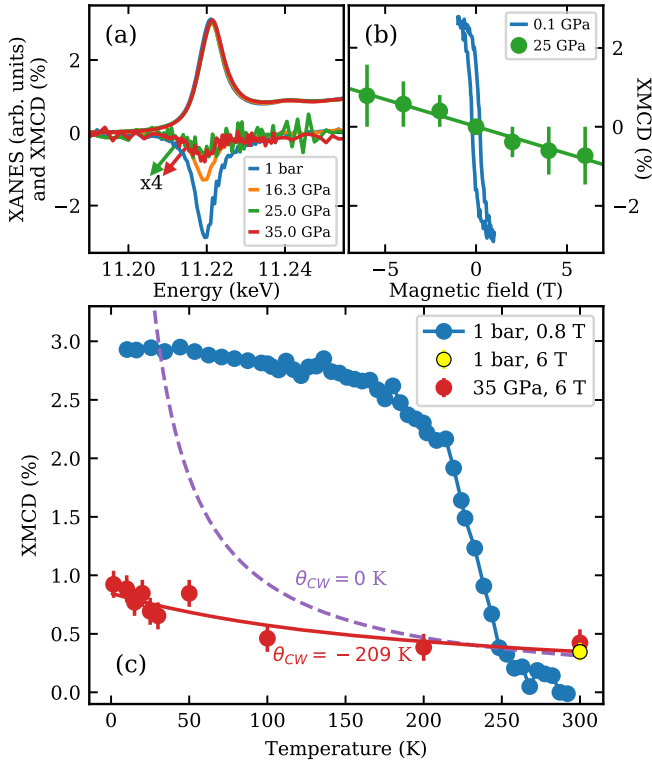
FIG. 3. (a) Ir L_3 x-ray absorption near edge structure (XANES) and XMCD spectra at selected pressures ($H = 1$ T, $T = 1.6$ K). The XMCD signal at 25 and 35 GPa are quadrupled for clarity. (b) Field-dependent XMCD at 0.1 GPa ($T = 6$ K) and 25 GPa ($T = 1.6$ K). (c) Temperature dependence of XMCD signal in the ordered (1 bar) and disordered (35 GPa) magnetic phases. A Curie-Weiss model yields $\theta_{CW} = -209$ K for the disordered phase (see Supplemental Material for additional details [44]). The susceptibility of an uncorrelated (Curie) paramagnet is shown with dashed lines. In a 6 T field, the susceptibility of the thermally disordered phase at ambient pressure ($T = 300 > T_N = 240$ K) is similar to that of the quantum disordered phase.

above, if the in-plane exchange interactions were undisturbed, such a large field would have induced magnetic ordering and a sizable W-FM response comparable to the response at ambient pressure (a 3.0% XMCD signal at the Ir L_3 edge corresponds to 0.05 μ_B/Ir [58]). A fit to a Curie-Weiss law yields $\theta_{CW} = -209(40)$ K and an effective moment of 1.45(7)μ_B [44]. The magnitude of the effective moment is close to the theoretical value for $J = \frac{1}{2}$ Ir^{4+} ions in the strong spin-orbit coupling limit [65]. The large negative value of θ_{CW} indicates strong local AFM correlations and a high degree of frustration in the intralayer coupling between localized Ir moments, even at $T = 1.6$ K ($f = |\theta_{CW}|/T_{min} \sim 140$ [19]). Note that a Curie paramagnet with no local exchange correlations would have resulted in $\times 15$–20 larger XMCD signal at 6 T, 1.6 K (local Ir moment is in the $\sim$0.25–0.35 μ_B range as determined by neutron scattering measurements [39]). Although the strength of local exchange interactions is comparable to that in the thermally induced paramagnetic state of Sr$_2$IrO$_4$ at ambient

pressure, $\theta_{CW} = +236$ K [60], the sign of local exchange interactions is opposite between these two phases, pointing to their distinct nature. The disordered magnetic state at high pressure is also distinct from typical disordered states obtained by doping the IrO$_2$ layers. For example, 3% Tb doping destroys magnetic order but yields a negligible $\theta_{CW} = -1.5$ K [66]. The dramatic degree of magnetic frustration in the presence of strong exchange interactions suggests that Sr-214 is a quantum paramagnet above 17–20 GPa.

The field-dependent XMCD signal in the high-pressure phase is displayed in Fig. 3(b). Both remanence and coercivity collapse, and a linear field dependence with no obvious discontinuities is observed. In general, the latter would suggest an ungapped quantum paramagnet, e.g., as a result of D-M interactions rooted in spin-orbit coupling mixing singlet and triplet states. However, while the full spin Hamiltonian of Sr-214 at ambient pressure can be mapped to SU(2) symmetry by a local rotation [9,29,67], the coupling of magnetic moments to an external magnetic field involves a nontrivial g tensor so that a measurement of the uniform spin susceptibility maps to a measurement of a linear combination of $Q = 0$ and $Q = (\pi, \pi)$ susceptibilities [9]. The nonzero $Q = (\pi, \pi)$ component would give a nonzero magnetic susceptibility even in the presence of a gap, so our data cannot rule out a gapped quantum paramagnet.

We now discuss possible routes to quantum paramagnetism in compressed Sr$_2$IrO$_4$. At ambient pressure, the dispersive magnetic excitations of Sr-214 have been measured by resonant inelastic x-ray scattering (RIXS) [28] and fit to an isotropic Heisenberg model of interacting isospins with exchange constants $J_1 = 60$, $J_2 = -20$, and $J_3 = 15$ meV. This fit neglects ring exchange J_r [68], which, like a negative J_2, results in downward dispersion from $Q = (\pi, 0)$ to $Q = [(\pi/2), (\pi/2)]$. Hence the values of J_2, J_3, and J_r are not unequivocally known and could provide a path to frustration. Nevertheless, taken at face value, the reported exchange constants at ambient pressure correctly predict a Néel phase within the $J_1 - J_2 - J_3$ model [26] and place Sr-214 in close proximity to a classical critical phase boundary $J_3 = 0.5|J_2 - 0.5J_1|$ near which quantum fluctuations can drive quantum paramagnetism [69]. It is thus plausible to conclude that a pressure-driven increase in orbital overlap and exchange interactions [70] pushes Sr-214 toward this phase boundary and quantum paramagnetism, with predictions including columnar and plaquette valence bond solids (VBSs) and spin-liquid phases [22,24]. Note that the columnar VBS breaks in-plane lattice translational symmetry, an effect not detected within the accuracy of previous powder [58,59] or current single crystal diffraction measurements. It remains to be seen whether realistic Hamiltonians for exchange correlations between $J_{eff} = \frac{1}{2}$ moments at high pressure can stabilize a quantum paramagnetic phase. In particular, the role of J_r in Sr-214

needs to be experimentally and theoretically clarified, as such exchange may also lead to quantum criticality [71,72]. Measuring the spectrum of magnetic excitations of Sr-214 at high pressure remains critical; not only to determine changes in the exchange constants, but also to verify if the isotropic Heisenberg model remains a valid approximation.

In conclusion, we show a remarkable response of magnetic interactions in Sr_2IrO_4 to compression. Pressures of a few GPa alter the interplanar magnetic exchange and drive a magnetic crossover that mimics that observed under a magnetic field at ambient pressure [5]. More importantly, higher pressures modify the intraplanar exchange between $J_{eff} = \frac{1}{2}$ isospins, leading to a highly frustrated magnetic state ($f \sim 140$) and possible emergence of quantum paramagnetism. This frustration is likely driven by a pressure-induced enhancement of J_2, J_3, and/or J_r exchange interactions relative to J_1, emphasizing the importance of exchange pathways beyond first neighbors in square lattices with extended $5d$ orbitals. In addition to opening exciting questions on the detailed nature of the magnetic state of Sr-214 at high pressures, these results raise the prospect of tuning other $5d$-based systems into emergent phases. For instance, a recent work in the double-layer $Sr_3Ir_2O_7$ has provided evidence for a magnetic phase transition around 15 GPa, above which the system is argued to be in a frustrated paramagnetic state [73]. Finally, advances in experimental techniques, such as RIXS [74,75] and nuclear resonant scattering [76], are required to probe magnetic excitations and short-range spin correlations in iridates at pressures of tens of GPa and beyond in order to provide deeper insight into the nature of quantum paramagnetic phases.

*haskel@anl.gov
†gfabbris@anl.gov

[1] S. H. Chun, J.-W. Kim, J. Kim, H. Zheng, C. C. Stoumpos, C. D. Malliakas, J. F. Mitchell, K. Mehlawat, Y. Singh, Y. Choi, T. Gog, A. Al-Zein, M. Moretti Sala, M. Krisch, J. Chaloupka, G. Jackeli, G. Khaliullin, and B. J. Kim, Direct evidence for dominant bond-directional interactions in a honeycomb lattice iridate Na_2IrO_3, Nat. Phys. **11**, 462 (2015).

[2] E. Lefrançois, V. Simonet, R. Ballou, E. Lhotel, A. Hadj-Azzem, S. Kodjikian, P. Lejay, P. Manuel, D. Khalyavin, and L. C. Chapon, Anisotropy-Tuned Magnetic Order in Pyrochlore Iridates, Phys. Rev. Lett. **114**, 247202 (2015).

[3] D. Pesin and L. Balents, Mott physics and band topology in materials with strong spinorbit interaction, Nat. Phys. **6**, 376 (2010).

[4] K. A. Modic, T. E. Smidt, I. Kimchi, N. P. Breznay, A. Biffin, S. Choi, R. D. Johnson, R. Coldea, P. Watkins-Curry, G. T. McCandless, J. Y. Chan, F. Gandara, Z. Islam, A. Vishwanath, A. Shekhter, R. D. McDonald, and J. G. Analytis, Realization of a three-dimensional spinanisotropic harmonic honeycomb iridate, Nat. Commun. **5**, 4203 (2014).

[5] B. J. Kim, H. Ohsumi, T. Komesu, S. Sakai, T. Morita, H. Takagi, and T. Arima, Phase-sensitive observation of a spin-orbital Mott state in Sr_2IrO_4, Science **323**, 1329 (2009).

[6] B. J. Kim, H. Jin, S. J. Moon, J.-Y. Kim, B.-G. Park, C. S. Leem, J. Yu, T. W. Noh, C. Kim, S.-J. Oh, J.-H. Park, V. Durairaj, G. Cao, and E. Rotenberg, Novel $J_{eff} = 1/2$ Mott State Induced by Relativistic Spin-Orbit Coupling in Sr_2IrO_4, Phys. Rev. Lett. **101**, 076402 (2008).

[7] Y. K. Kim, N. H. Sung, J. D. Denlinger, and B. J. Kim, Observation of a d-wave gap in electron-doped Sr_2IrO_4, Nat. Phys. **12**, 37 (2016).

[8] A. de la Torre, S. McKeown Walker, F. Y. Bruno, S. Riccó, Z. Wang, I. Gutierrez Lezama, G. Scheerer, G. Giriat, D. Jaccard, C. Berthod, T. K. Kim, M. Hoesch, E. C. Hunter, R. S. Perry, A. Tamai, and F. Baumberger, Collapse of the Mott Gap and Emergence of a Nodal Liquid in Lightly Doped Sr_2IrO_4, Phys. Rev. Lett. **115**, 176402 (2015).

[9] F. Wang and T. Senthil, Twisted Hubbard Model for Sr_2IrO_4: Magnetism and Possible High Temperature Superconductivity, Phys. Rev. Lett. **106**, 136402 (2011).

[10] A. Shitade, H. Katsura, J. Kuneš, X.-L. Qi, S.-C. Zhang, and N. Nagaosa, Quantum Spin Hall Effect in a Transition Metal Oxide Na_2IrO_3, Phys. Rev. Lett. **102**, 256403 (2009).

[11] G. Jackeli and G. Khaliullin, Mott Insulators in the Strong Spin-Orbit Coupling Limit: From Heisenberg to a Quantum Compass and Kitaev Models, Phys. Rev. Lett. **102**, 017205 (2009).

[12] L. C. Chapon and S. W. Lovesey, The magnetic motif and the wavefunction of Kramers ions in strontium iridate (Sr_2IrO_4), J. Phys. Condens. Matter **23**, 252201 (2011).

[13] R. Arita, J. Kuneš, A. V. Kozhevnikov, A. G. Eguiluz, and M. Imada, Ab Initio Studies on the Interplay Between Spin-Orbit Interaction and Coulomb Correlation in Sr_2IrO_4 and Ba_2IrO_4, Phys. Rev. Lett. **108**, 086403 (2012).

[14] J. Bertinshaw, Y. K. Kim, G. Khaliullin, and B. J. Kim, Square Lattice Iridates, Annu. Rev. Condens. Matter Phys. **10**, 315 (2019).

[15] T. Takayama, A. Kato, R. Dinnebier, J. Nuss, H. Kono, L. S. I. Veiga, G. Fabbris, D. Haskel, and H. Takagi, Hyperhoneycomb Iridate $\beta - Li_2IrO_3$ as a Platform for Kitaev Magnetism, Phys. Rev. Lett. **114**, 077202 (2015).

[16] I. Kimchi and A. Vishwanath, Kitaev-Heisenberg models for iridates on the triangular, hyperkagome, kagome, fcc, and pyrochlore lattices, Phys. Rev. B **89**, 014414 (2014).

[17] Y. Shimizu, K. Miyagawa, K. Kanoda, M. Maesato, and G. Saito, Spin Liquid State in an Organic Mott Insulator with a Triangular Lattice, Phys. Rev. Lett. **91**, 107001 (2003).

[18] T. Takayama, A. Yaresko, A. Matsumoto, J. Nuss, K. Ishii, M. Yoshida, J. Mizuki, and H. Takagi, Spin-orbit coupling

induced semi-metallic state in the 1/3 hole-doped hyper-kagome $Na_3Ir_3O_8$, Sci. Rep. **4,** 6818 (2015).

[19] L. Balents, Spin liquids in frustrated magnets, Nature (London) **464,** 199 (2010).

[20] A. Yu. Kitaev, Fault-tolerant quantum computation by anyons, Ann. Phys. (Amsterdam) **303,** 2 (2003).

[21] F. Figueirido, A. Karlhede, S. Kivelson, S. Sondhi, M. Rocek, and D. S. Rokhsar, Exact diagonalization of finite frustrated spin-$\frac{1}{2}$ Heisenberg models, Phys. Rev. B **41,** 4619 (1990).

[22] N. Read and S. Sachdev, Large-N Expansion for Frustrated Quantum Antiferromagnets, Phys. Rev. Lett. **66,** 1773 (1991).

[23] J. Ferrer, Spin-liquid phase for the frustrated quantum Heisenberg antiferromagnet on a square lattice, Phys. Rev. B **47,** 8769 (1993).

[24] M. Mambrini, A. Läuchli, D. Poilblanc, and F. Mila, Plaquette valence-bond crystal in the frustrated Heisenberg quantum antiferromagnet on the square lattice, Phys. Rev. B **74,** 144422 (2006).

[25] J. Reuther, P. Wölfle, R. Darradi, W. Brenig, M. Arlego, and J. Richter, Quantum phases of the planar antiferromagnetic $J_1 - J_2 - J_3$ Heisenberg model, Phys. Rev. B **83,** 064416 (2011).

[26] B. Danu, G. Nambiar, and R. Ganesh, Extended degeneracy and order by disorder in the square lattice $J_1 - J_2 - J_3$ model, Phys. Rev. B **94,** 094438 (2016).

[27] P. W. Anderson, Resonating valence bond state in La_2CuO_4 and superconductivity, Science **235,** 1196 (1987).

[28] J. Kim, D. Casa, M. H. Upton, T. Gog, Y.-J. Kim, J. F. Mitchell, M. van Veenendaal, M. Daghofer, J. van den Brink, G. Khaliullin, and B. J. Kim, Magnetic Excitation Spectra of Sr_2IrO_4 Probed by Resonant Inelastic X-Ray Scattering: Establishing Links to Cuprate Superconductors, Phys. Rev. Lett. **108,** 177003 (2012).

[29] L. Hao, D. Meyers, H. Suwa, J. Yang, C. Frederick, T. R. Dasa, G. Fabbris, L. Horak, D. Kriegner, Y. Choi, J.-W. Kim, D. Haskel, P. J. Ryan, H. Xu, C. D. Batista, M. P. M. Dean, and J. Liu, Giant magnetic response of a two-dimensional antiferromagnet, Nat. Phys. **14,** 806 (2018).

[30] S. A. Kivelson, D. S. Rokhsar, and J. P. Sethna, Topology of the resonating valence-bond state: Solitons and high-T_c superconductivity, Phys. Rev. B **35,** 8865 (1987).

[31] T. Senthil and M. P. A. Fisher, Z_2 gauge theory of electron fractionalization in strongly correlated systems, Phys. Rev. B **62,** 7850 (2000).

[32] N. Read and S. Sachdev, Valence-Bond and Spin-Peierls Ground States of Low-Dimensional Quantum Antiferromagnets, Phys. Rev. Lett. **62,** 1694 (1989).

[33] M. Majumder, R. S. Manna, G. Simutis, J. C. Orain, T. Dey, F. Freund, A. Jesche, R. Khasanov, P. K. Biswas, E. Bykova, N. Dubrovinskaia, L. S. Dubrovinsky, R. Yadav, L. Hozoi, S. Nishimoto, A. A. Tsirlin, and P. Gegenwart, Breakdown of Magnetic Order in the Pressurized Kitaev Iridate $\beta - Li_2IrO_3$, Phys. Rev. Lett. **120,** 237202 (2018).

[34] N. P. Breznay, A. Ruiz, A. Frano, W. Bi, R. J. Birgeneau, D. Haskel, and J. G. Analytis, Resonant x-ray scattering reveals possible disappearance of magnetic order under hydrostatic pressure in the Kitaev candidate $\gamma - Li_2IrO_3$, Phys. Rev. B **96,** 020402(R) (2017).

[35] L. S. I. Veiga, M. Etter, K. Glazyrin, F. Sun, C. A. Escanhoela, G. Fabbris, J. R. L. Mardegan, P. S. Malavi, Y. Deng, P. P. Stavropoulos, H.-Y. Kee, W. G. Yang, M. van Veenendaal, J. S. Schilling, T. Takayama, H. Takagi, and D. Haskel, Pressure tuning of bond-directional exchange interactions and magnetic frustration in the hyperhoneycomb iridate Li_2IrO_3, Phys. Rev. B **96,** 140402(R) (2017).

[36] V. Hermann, M. Altmeyer, J. Ebad-Allah, F. Freund, A. Jesche, A. A. Tsirlin, M. Hanfland, P. Gegenwart, I. I. Mazin, D. I. Khomskii, R. Valentí, and C. A. Kuntscher, Competition between spin-orbit coupling, magnetism, and dimerization in the honeycomb iridates: $\alpha - Li_2IrO_3$ under pressure, Phys. Rev. B **97,** 020104(R) (2018).

[37] T. Takayama, A. Krajewska, A. S. Gibbs, A. N. Yaresko, H. Ishii, H. Yamaoka, K. Ishii, N. Hiraoka, N. P. Funnell, C. L. Bull, and H. Takagi, Pressure-induced collapse of the spin-orbital Mott state in the hyperhoneycomb iridate $\beta - Li_2IrO_3$, Phys. Rev. B **99,** 125127 (2019).

[38] L. S. I. Veiga, K. Glazyrin, G. Fabbris, C. D. Dashwood, J. G. Vale, H. Park, M. Etter, T. Irifune, S. Pascarelli, D. F. McMorrow, T. Takayama, H. Takagi, and D. Haskel, Pressure-induced structural dimerization in the hyperhoneycomb iridate $\beta - Li_2IrO_3$ at low temperatures, Phys. Rev. B **100,** 064104 (2019).

[39] F. Ye, S. Chi, B. C. Chakoumakos, J. A. Fernandez-Baca, T. Qi, and G. Cao, Magnetic and crystal structures of Sr_2IrO_4: A neutron diffraction study, Phys. Rev. B **87,** 140406(R) (2013).

[40] I. Dzyaloshinsky, A thermodynamic theory of weak ferromagnetism of antiferromagnetics, J. Phys. Chem. Solids **4,** 241 (1958).

[41] T. Moriya, Anisotropic superexchange interaction and weak ferromagnetism, Phys. Rev. **120,** 91 (1960).

[42] S. Calder, D. M. Pajerowski, M. B. Stone, and A. F. May, Spin-gap and two-dimensional magnetic excitations in Sr_2IrO_4, Phys. Rev. B **98,** 220402(R) (2018).

[43] G. Cao, J. Bolivar, S. McCall, J. E. Crow, and R. P. Guertin, Weak ferromagnetism, metal-to-nonmetal transition, and negative differential resistivity in single-crystal Sr_2IrO_4, Phys. Rev. B **57,** R11039 (1998).

[44] See Supplemental Material at http://link.aps.org/supplemental/10.1103/PhysRevLett.124.067201 for experimental details, information on the IrO_6 octahedral rotations, and crystal strain at high pressures, as well as descriptions on how T_N and the magnetic susceptibility were extracted from the XMCD data, which includes Refs. [15,39,45–60].

[45] A. G. Gavriliuk, A. A. Mironovich, and V. V. Struzhkin, Miniature diamond anvil cell for broad range of high pressure measurements, Rev. Sci. Instrum. **80,** 043906 (2009).

[46] Y. Feng, R. Jaramillo, J. Wang, Y. Ren, and T. F. Rosenbaum, Invited Article: High-pressure techniques for condensed matter physics at low temperature, Rev. Sci. Instrum. **81,** 041301 (2010).

[47] W. B. Holzapfel, M. Harwig, and W. Sievers, Equations of state for Cu, Ag, and Au for wide ranges in temperature and pressure up to 500 GPa and above, J. Phys. Chem. Ref. Data **30,** 515 (2001).

[48] M. Suzuki, N. Kawamura, M. Mizumaki, A. Urata, H. Maruyama, S. Goto, and T. Ishikawa, Helicity-modulation technique using diffractive phase retarder for measurements

of x-ray magnetic circular dichroism, Jpn. J. Appl. Phys. **37,** L1488 (1998).

[49] D. Haskel, Y. C. Tseng, J. C. Lang, and S. Sinogeikin, Instrument for x-ray magnetic circular dichroism measurements at high pressures, Rev. Sci. Instrum. **78,** 083904 (2007).

[50] D. Haskel, Y. C. Tseng, N. M. Souza-Neto, J. C. Lang, S. Sinogeikin, Ya Mudryk, K. A. Gschneidner, and V. K. Pecharsky, Magnetic spectroscopy at high pressures using x-ray magnetic circular dichroism, High Press. Res. **28,** 185 (2008).

[51] K. Syassen, Ruby under pressure, High Press. Res. **28,** 75 (2008).

[52] M. K. Crawford, M. A. Subramanian, R. L. Harlow, J. A. Fernandez-Baca, Z. R. Wang, and D. C. Johnston, Structural and magnetic studies of Sr_2IrO_4, Phys. Rev. B **49,** 9198 (1994).

[53] Q. Huang, J. L. Soubeyroux, O. Chmaissem, I. Natali Sora, A. Santoro, R. J. Cava, J. J. Krajewski, and W. F. Peck, Neutron powder diffraction study of the crystal structures of Sr_2RuO_4 and Sr_2IrO_4 at room temperature and at 10 K, J. Solid State Chem. **112,** 355 (1994).

[54] B. T. Thole, P. Carra, F. Sette, and G. van der Laan, X-Ray Circular Dichroism as a Probe of Orbital Magnetization, Phys. Rev. Lett. **68,** 1943 (1992).

[55] P. Carra, B. T. Thole, M. Altarelli, and X. Wang, X-Ray Circular Dichroism and Local Magnetic Fields, Phys. Rev. Lett. **70,** 694 (1993).

[56] M. A. Laguna-Marco, D. Haskel, N. Souza-Neto, J. C. Lang, V. V. Krishnamurthy, S. Chikara, G. Cao, and M. van Veenendaal, Orbital Magnetism and Spin-Orbit Effects in the Electronic Structure of $BaIrO_3$, Phys. Rev. Lett. **105,** 216407 (2010).

[57] M. Ge, T. F. Qi, O. B. Korneta, D. E. De Long, P. Schlottmann, W. P. Crummett, and G. Cao, Lattice-driven magnetoresistivity and metal-insulator transition in single-layered iridates, Phys. Rev. B **84,** 100402(R) (2011).

[58] D. Haskel, G. Fabbris, M. Zhernenkov, P. P. Kong, C. Q. Jin, G. Cao, and M. van Veenendaal, Pressure Tuning of the Spin-Orbit Coupled Ground State in Sr_2IrO_4, Phys. Rev. Lett. **109,** 027204 (2012).

[59] K. Samanta, F. M. Ardito, N. M. Souza-Neto, and E. Granado, First-order structural transition and pressure-induced lattice/phonon anomalies in Sr_2IrO_4, Phys. Rev. B **98,** 094101 (2018).

[60] S. Chikara, O. Korneta, W. P. Crummett, L. E. DeLong, P. Schlottmann, and G. Cao, Giant magnetoelectric effect in the $J_{eff} = \frac{1}{2}$ Mott insulator Sr_2IrO_4, Phys. Rev. B **80,** 140407(R) (2009).

[61] S. Boseggia, R. Springell, H. C. Walker, H. M. Rønnow, Ch. Rüegg, H. Okabe, M. Isobe, R. S. Perry, S. P. Collins, and D. F. McMorrow, Robustness of Basal-Plane Antiferromagnetic Order and the $J_{eff} = \frac{1}{2}$ State in Single-Layer Iridate Spin-Orbit Mott Insulators, Phys. Rev. Lett. **110,** 117207 (2013).

[62] S. Moser, L. Moreschini, A. Ebrahimi, B. Dalla Piazza, M. Isobe, H. Okabe, J. Akimitsu, V. V. Mazurenko, K. S. Kim, A. Bostwick, E. Rotenberg, J. Chang, H. M. Rønnow, and M. Grioni, The electronic structure of the high-symmetry perovskite iridate Ba_2IrO_4, New J. Phys. **16,** 013008 (2014).

[63] S. Calder, G.-X. Cao, M. D. Lumsden, J. W. Kim, Z. Gai, B. C. Sales, D. Mandrus, and A. D. Christianson, Magnetic structural change of Sr_2IrO_4 upon Mn doping, Phys. Rev. B **86,** 220403(R) (2012).

[64] D. A. Zocco, J. J. Hamlin, B. D. White, B. J. Kim, J. R. Jeffries, S. T. Weir, Y. K. Vohra, J. W. Allen, and M. B. Maple, Persistent non-metallic behavior in Sr_2IrO_4 and $Sr_3Ir_2O_7$ at high pressures, J. Phys. Condens. Matter **26,** 255603 (2014).

[65] Brendan F. Phelan, Jason Krizan, Weiwei Xie, Quinn Gibson, and R. J. Cava, New material for probing spin-orbit coupling in iridates, Phys. Rev. B **91,** 155117 (2015).

[66] J. C. Wang, S. Aswartham, F. Ye, J. Terzic, H. Zheng, D. Haskel, S. Chikara, Y. Choi, P. Schlottmann, R. Custelcean, S. J. Yuan, and G. Cao, Decoupling of the antiferromagnetic and insulating states in Tb-doped Sr_2IrO_4, Phys. Rev. B **92,** 214411 (2015).

[67] L. Shekhtman, O. Entin-Wohlman, and A. Aharony, Moriya's Anisotropic Superexchange Interaction, Frustration, and Dzyaloshinsky's Weak Ferromagnetism, Phys. Rev. Lett. **69,** 836 (1992).

[68] R. Coldea, S. M. Hayden, G. Aeppli, T. G. Perring, C. D. Frost, T. E. Mason, S.-W. Cheong, and Z. Fisk, Spin Waves and Electronic Interactions in La_2CuO_4, Phys. Rev. Lett. **86,** 5377 (2001).

[69] L. Capriotti and S. Sachdev, Low-Temperature Broken-Symmetry Phases of Spiral Antiferromagnets, Phys. Rev. Lett. **93,** 257206 (2004).

[70] Evidence for enhanced overlap of 5d orbitals under pressure comes from electrical resistance measurements, which show a continuous reduction of the Mott gap to at least 20 GPa [58,64].

[71] K. Misumi, K. Seki, and Y. Ohta, Spin excitations in the Square-Lattice Heisenberg model with ring-exchange interactions, J. Phys. Soc. Jpn. **014021,** 2 (2014).

[72] C. B. Larsen, A. T. Rømer, S. Janas, F. Treue, B. Mønsted, N. E. Shaik, H. M. Rønnow, and K. Lefmann, Exact diagonalization study of the Hubbard-parametrized four-spin ring exchange model on a square lattice, Phys. Rev. B **99,** 054432 (2019).

[73] J. Zhang, D. Yan, S. Yesudhas, H. Deng, H. Xiao, B. Chen, R. Sereika, X. Yin, C. Yi, Y. Shi, Z. Liu, E. M. Pärschke, C.-C. Chen, J. Chang, Y. Ding, and H.-k. Mao, Lattice frustration in spin-orbit Mott insulator $Sr_3Ir_2O_7$ at high pressure, npj Quantum Mater. **4,** 23 (2019).

[74] M. Rossi, C. Henriquet, J. Jacobs, C. Donnerer, S. Boseggia, A. Al-Zein, R. Fumagalli, Y. Yao, J. G. Vale, E. C. Hunter, R. S. Perry, I. Kantor, G. Garbarino, W. Crichton, G. Monaco, D. F. McMorrow, M. Krisch, and M. M. Sala, Resonant inelastic x-ray scattering of magnetic excitations under pressure, J. Synchrotron Radiat. **26,** 1725 (2019).

[75] J. Kim, Advances in high-resolution RIXS for the study of excitation spectra under high pressure, High Press. Res. **36,** 391 (2016).

[76] P. Alexeev, O. Leupold, I. Sergueev, M. Herlitschke, D. F. McMorrow, R. S. Perry, E. C. Hunter, R. Röhlsberger, and H.-C. Wille, Nuclear resonant scattering from ^{193}Ir as a probe of the electronic and magnetic properties of iridates, Sci. Rep. **9,** 5097 (2019).

[77] M. Rivers, V. Prakapenka, A. Kubo, C. Pullins, C. Holl, and S. Jacobsen, The COMPRES/GSECARS gas-loading system for diamond anvil cells at the Advanced Photon Source, High Press. Res. **28,** 273 (2008).